Computational Mechanics 16 (1995) 1–10 © Springer-Verlag 1995

Computational study of flow past a cylinder with combined in-line and transverse oscillation

D. Karanth, G. W. Rankin, K. Sridhar

Abstact A computational study of the two dimensional flow past an oscillating cylinder is carried out using vorticity and stream function as the dependent variables. With the use of a log-polar coordinate transformation, the nondimensional vorticity transport equations in a non-inertial frame attached to the cylinder are solved using the ADI and SLOR finite difference schemes. The effects of combined in-line and transverse oscillation of the cylinder in the "lock-in" range of frequency on the time history of the drag and lift are investigated at a Reynolds number of 100. In addition, the influence of position amplitude of the cylinder's transverse oscillation on the lock-in range of frequency, mean drag, amplitude of drag and maximum lift is studied. The time histories of drag and lift forces in the case of combined oscillation are compared with the cases of the cylinder oscillating in the in-line and transverse directions separately. The dominant frequency components in the drag and the lift variations are determined using a Fourier frequency analysis.

List of symbols

a	transformation parameter
a_x, a_y	position amplitudes of forced cylinder oscillation in the in-line and transverse directions, respectively, $A_x'T_x/2\pi$, $A_y'T_y/2\pi$
A_x', A_y'	Velocity amplitudes of forced cylinder oscillation in the in-line and transverse directions, respectively
A_x, A_y	nondimensional velocity amplitudes of forced cylinder oscillation in the in-line and transverse directions, respectively, A_x'/U_∞, A_y'/U_∞
Cd	nondimensional drag force, $d/\rho U_\infty^2 R$
Cd_m	mean drag force
Cd_{amp}	amplitude of drag force
Cl	nondimensional lift force, $l/\rho U_\infty^2 R$
Cl_{max}	maximum lift force
d	drag force
D	diameter of the cylinder
F_n	nondimensional natural shedding frequency (Strouhal number), D/T_nU_∞
F_x, F_y	nondimensional forced frequency parameters in the in-line and transverse directions, respectively, D/T_xU_∞, D/T_yU_∞
l	lift force
p	pressure
p_∞	free stream pressure
P	nondimensional pressure, $(p-p_\infty)/\rho U_\infty^2$
PSD	Power spectral density
(r, θ)	radial and tangential coordinates in a frame of reference attached to the cylinder
R	radius of the cylinder
Re_D	Reynolds number based on cylinder diameter, $U_\infty D/\nu$
t	time
T_d	time delay
T_n	natural shedding period
T_x, T_y	period of forced oscillation in the in-line and transverse directions, respectively
U, V	nondimensional convective velocities in the ξ and η directions, respectively (Eq. 6)
U_∞	free stream velocity
v_r, v_θ	relative velocities in the r and θ directions, respectively
V_r, V_θ	nondimensional relative velocities in the r and θ directions, respectively, v_r/U_∞, v_θ/U_∞
(ξ, η)	nondimensional log-polar coordinates, $r/R = e^{a\xi}$, $\theta = a\eta$
ε	incident angle of the free stream velocity relative to the frame of reference attached to the cylinder
ν	kinematic viscosity of the fluid
ρ	density of the fluid
τ	nondimensional time, tU_∞/R
τ_d	nondimensional time delay, T_dU_∞/R
ϕ	phase difference between the transverse and in-line oscillation
ψ	stream function relative to the frame attached to the cylinder
Ψ	nondimensional stream function relative to the frame attached to the cylinder, ψ/rU_∞
ω	vorticity
Ω	nondimensional vorticity, $\omega R/U_\infty$

Communicated by S. N. Atluri, 20 October 1994

D. Karanth, G. W. Rankin, K. Sridhar
Department of Mechanical Engineering and Fluid Dynamics Research Institute, University of Windsor, Windsor, Ontario Canada, N9B 3P4

Correspondence to: G. W. Rankin

This research work was financially supported through a University of Windsor Postgraduate Scholarship and grants from the Natural sciences and Engineering Research Council of Canada (Grant Numbers: A-2190 and A-1403).

1 Introduction

Wakes behind bluff bodies are of major importance in engineering, primarily because of the associated drag, lift and energy loss. In addition, they are associated with flow induced

oscillation of a variety of cylindrical structures. Over a wide range of Reynolds numbers, vortex streets are formed in the wakes of the cylindrical bluff bodies. The vortices in the wake interact with the cylinder and induce oscillating lift and drag forces on the cylinder. The oscillation frequencies of the lift and drag forces are directly related to the vortex shedding frequency. The drag force oscillates at twice the vortex shedding frequency and the lift force oscillates at a frequency equal to the vortex shedding frequency. The incident flow may excite resonant oscillations if the cylinder is flexible.

The transverse oscillation of the cylinder with a frequency at or near the natural vortex shedding frequency results in an increase in the mean drag on the cylinder and causes the vortex shedding to occur at the frequency of cylinder oscillation. This type of fluid-structure interaction is known as "lock-in" or "synchronization" or "wake capture". Similarly, the in-line oscillation of the cylinder with a frequency at or near twice the natural vortex shedding frequency produces an increased lift amplitude and causes the vortex shedding to occur at half the frequency of the cylinder oscillation. Both the in-line and transverse oscillation of the cylinder within the respective lock-in frequency range, alter the phase, sequence and pattern of vortices in the wake and increase the vortex strength. In the case of flow induced oscillation, the position amplitude of the cylinder oscillation in the in-line direction is less than in the transverse direction. Lock-in occurs both with forced oscillation of the cylinder and flow induced oscillation of the cylinder.

There are several experimental investigations of cylinders oscillating in a direction in-line or transverse to that of the mean flow direction (Tanaka and Takahara (1969); Bublitz (1972); Tanida et al. (1973); Griffin and Ramberg (1974, 1976); Stansby (1976); Bearman and Obasaju (1989); Moe and Wu (1989)). Hurbult et al. (1982), were the first to carry out a numerical investigation of flow past an oscillating cylinder. They solved the governing equations in the primitive variable form in a non-inertial frame of reference using the Marker and Cell (MAC) method. Other numerical investigations (Chilukuri (1987); Tsuboi et al. (1988); Lecointe and Piquet (1989); Triantafyllou and Karniadakis (1989); Rao et al. (1992); Li et al. (1992); Mittal and Tezduyar (1992)) consider only the flow past a cylinder oscillating in the in-line or transverse directions separately. To the author's knowledge, no numerical or experimental investigation has been attempted for the case of flow past a cylinder with combined oscillation, i.e., the cylinder oscillating in the in-line and transverse directions simultaneously.

The primary objective of this study is to determine the effects of combined oscillation, in the lock in range of forcing frequencies, on the time histories of the lift and drag forces. The secondary objective is to investigate the influence of position amplitude of the cylinder's transverse oscillation on the lock-in range of frequency, mean drag, amplitude of drag and maximum lift. In addition, the independent effects of in-line and transverse lock-in cylinder oscillations will be considered. The non-dimensionalized vorticity transport equation in a non-inertial reference frame (attached to the cylinder) is solved in a rectangular grid based on log-polar coordinates (ξ, η). Finite difference simulations are conducted at a Reynolds number of 100. The position amplitude of the cylinder in the in-line direction is set equal to $0.2D$. In order to study the effect of position amplitude of oscillation in the transverse direction on the drag and lift forces, numerical experiments are conducted using values of $0.2D$, $0.4D$ and $0.8D$.

2 Governing equations and boundary conditions

After an alternating vortex street is formed in the wake, the cylinder is forced to oscillate sinusoidally with velocities, $A'_x \sin(2\pi\{t - T_d\}/T_x)$ and $A'_y \sin(2\pi\{t - T_d\}/T_y - \phi)$ in the in-line and transverse directions respectively, relative to the mean flow (Fig. 1). The phase difference ϕ between the in-line and transverse oscillations is set equal to zero in this study. The time delay T_d is the time allowed for the development of a stable alternating vortex street in the wake of a stationary cylinder. In order to achieve a fixed grid with respect to the cylinder, it is necessary to use a non-inertial reference frame attached to the cylinder. The governing equations for a two dimensional flow problem are the continuity and two momentum component equations. By introducing the stream function and vorticity into these equations, they can be simplified and reduced to two equations: the vorticity transport equations. In the case of an oscillating cylinder, the vorticity transport equations in a non-inertial reference frame retain the same form as in the inertial frame of reference and are given by

$$\frac{\partial \omega}{\partial t} + \frac{1}{r}\left[\frac{\partial}{\partial r}\left(\omega \frac{\partial \psi}{\partial \theta}\right) - \frac{\partial}{\partial \theta}\left(\omega \frac{\partial \psi}{\partial r}\right)\right] = \nu \nabla^2 \omega, \tag{1}$$

$$\omega = -\nabla^2 \psi, \tag{2}$$

where

$$\nabla^2 = \frac{\partial^2}{\partial r^2} + \frac{1}{r}\frac{\partial}{\partial r} + \frac{1}{r^2}\frac{\partial^2}{\partial \theta^2}.$$

The relative velocities in the radial and tangential directions are defined as

$$v_r = \frac{1}{r}\frac{\partial \psi}{\partial \theta}, \quad v_\theta = -\frac{\partial \psi}{\partial r}. \tag{3}$$

In order to achieve a more accurate numerical solution, it is essential to have a finer grid near the cylinder. This can be accomplished by the use of a log-polar coordinate transformation given by

$$r/R = e^{a\xi} \text{ and } \theta = a\eta, \tag{4}$$

where "a", the transformation parameter, is set equal to π in this study. This log-polar coordinate transformation allows us

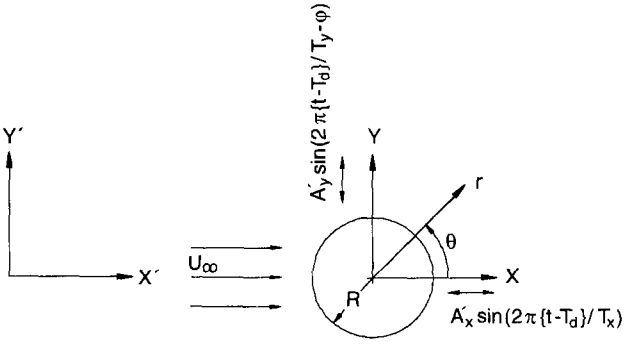

Fig. 1. Coordinate systems

to have a uniform grid in a transformed rectangular domain. After applying the log-polar coordinate transformation, the nondimensionalized vorticity transport equations are

$$g(\xi)\frac{\partial \Omega}{\partial \tau}+\frac{\partial}{\partial \xi}\left(\Omega\frac{\partial \Psi}{\partial \eta}\right)-\frac{\partial}{\partial \eta}\left(\Omega\frac{\partial \Psi}{\partial \xi}\right)=\frac{2}{Re}\nabla^2\Omega, \tag{5}$$

$$g(\xi)\Omega=-\nabla^2\Psi, \tag{6}$$

where

$$g(\xi)=a^2e^{2a\xi},$$

$$\nabla^2=\frac{\partial^2}{\partial \xi^2}+\frac{\partial^2}{\partial \eta^2},$$

and the nondimensional convective velocities in ξ and η directions are given by

$$U=\frac{\partial \Psi}{\partial \eta}, \quad V=-\frac{\partial \Psi}{\partial \xi}. \tag{7}$$

The nondimensional relative velocities in the radial and tangential directions are then given by

$$V_r=\frac{v_r}{U_\infty}=\frac{U}{\sqrt{g(\xi)}}, \quad V_\theta=\frac{v_\theta}{U_\infty}=\frac{V}{\sqrt{g(\xi)}}. \tag{8}$$

The boundary conditions on the cylinder surface are given by

$$\Psi=\frac{\partial \Psi}{\partial \xi}=0, \quad \Omega=-\frac{1}{a^2}\left(\frac{\partial^2\Psi}{\partial \xi^2}\right)_0 \quad \text{on } \xi=0. \tag{9}$$

The assumption of $\Psi=0$ on the body surface is valid as the defined stream function is relative to the coordinate frame attached to the cylinder.

The time-dependent far-field boundary condition for the relative stream function is obtained by using the potential flow solution:

$$\Psi=2\sqrt{[1-A_x\sin(\pi(\tau-\tau_d)F_x)]^2+[A_y\sin(\pi(\tau-\tau_d)F_y-\phi)]^2}\cdot\sinh(a\xi_\infty)\sin(a\eta-\varepsilon), \tag{10}$$

where

$$\varepsilon=\tan^{-1}\left[\frac{-A_y\sin(\pi(\tau-\tau_d)F_y-\phi)}{1-A_x\sin(\pi(\tau-\tau_d)F_x)}\right].$$

The far-field vorticity boundary conditions are

$$\left[g(\xi)\frac{\partial \Omega}{\partial \tau}+\frac{\partial}{\partial \xi}\left(\Omega\frac{\partial \Psi}{\partial \eta}\right)-\frac{\partial}{\partial \eta}\left(\Omega\frac{\partial \Psi}{\partial \xi}\right)\right]_{\xi_\infty}=0, \quad 0<\eta<\tfrac{1}{2}, \quad \tfrac{3}{2}<\eta<2, \tag{11}$$

and

$$\Omega=0, \quad \tfrac{1}{2}\leqq\eta\leqq\tfrac{3}{2}.$$

The time-dependent downstream boundary condition is called the "radiant-Sommerfeld like" condition where the diffusion of vorticity is neglected (Ta Phuoc Loc and Bouard (1985)). Upstream of the cylinder, the irrotational boundary condition is always valid.

3 Computational procedure

Figure 2 shows the computational domain in the (ξ,η) coordinate system. On the boundaries: $\eta=0$ and $\eta=2$, a cyclic boundary condition is imposed on the dependent variables. The vorticity transport equations are solved numerically using the ADI scheme. The time derivative is approximated using forward differencing and the diffusion terms are calculated using the central differencing scheme. The velocities in the convective terms are calculated using the fourth order accurate Hermitian relation. The vorticity boundary condition on the cylinder can be approximated numerically in different ways. In this study, a second order accurate cubic polynomial approximation is used. The Poisson equation is solved iteratively using the SLOR scheme. An optimum relaxation coefficient (Son and Hanratty (1969)) is used to enhance the convergence rate. The numerical solution obtained is first order accurate in time and second order accurate in space. The nondimensional time step and the grid size are taken to be 0.01 and 101 × 121, respectively. The far-field boundary was located at 23.24R ($\xi_\infty=1$). In the initial stage of simulation, the cylinder was rotated counterclockwise and then clockwise for a small duration of time with a constant angular velocity. This numerical triggering procedure is required to initiate the alternating vortex street (Jordan and Fromm (1972)). At every time step, the vorticity in the far-field was calculated using the finite difference form of equation (11). The nondimensional time of 40 (τ_d) was allowed for the development of an alternating vortex street. Numerical simulations were carried out for the stationary cylinder case and for the cylinder oscillating in the in-line and transverse directions separately as well as the case of a combined oscillation in the in-line and transverse directions. The nondimensional pressure distribution on the cylinder was obtained by integrating the following equation:

$$\frac{\partial P}{\partial \eta}=\frac{2}{Re_D}\left(\frac{\partial \Omega}{\partial \xi}\right)_{\xi=0}-a\pi\{-A_xF_x\cos(\pi(\tau-\tau_d)F_x)\sin(a\eta)+A_yF_y\cos(\pi(\tau-\tau_d)F_y-\phi)\cos(a\eta)\}. \tag{12}$$

In order to reduce the error in the computed pressure values between the starting point ($\eta=1$) and the ending point ($\eta=1$), the vorticity gradient on the cyinder in the ξ direction is

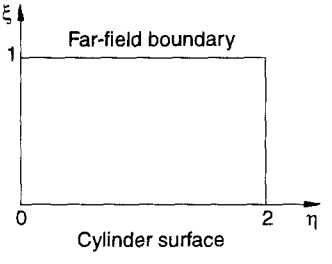

Fig. 2. Computational domain

calculated using a fourth order accurate finite difference form. The drag and lift coefficients were calculated using the following expressions:

$$C_d = -\int_0^{2\pi} P\cos\theta\, d\theta - \frac{2}{Re_D}\int_o^{2\pi} \Omega\sin\theta\, d\theta, \tag{13}$$

$$C_l = -\int_0^{2\pi} P\sin\theta\, d\theta + \frac{2}{Re_D}\int_o^{2\pi} \Omega\cos\theta\, d\theta. \tag{14}$$

4
Numerical results

Excluding the initial transients associated with the start-up of the cylinder oscillation, the results are given in the form of mean drag, amplitude of the drag, maximum lift and power spectrum at various conditions. The time history of the drag and lift are shown at $F_x = 2F_n$, i.e., the forcing frequency in the in-line direction equal to twice the Strouhal frequency and $F_y = F_n$, i.e., the forcing frequency in the transverse direction equal to the Strouhal frequency. The power spectrum of the drag is obtained by taking the FFT of the drag variation minus the mean drag. The power spectrum of the lift is obtained by taking the FFT of the lift variation.

Figure 3 shows the time history of the drag and lift for a stationary cylinder at a Reynolds number of 100. Note that the drag is oscillating at twice the Strouhal frequency with a very small amplitude. The lift is oscillating with a frequency equal to the Strouhal frequency. The power spectra (Fig. 4) shows the dominant frequencies in the drag and lift variation.

4.1
Validation

In order to validate the numerical model, simulations were run at a Reynolds number of 80. The predicted Strouhal numbers at Reynolds number of 80 and 100 are compared with the experimental values given by Roshko (1955). The numerical results obtained for the case of flow past a stationary cylinder and for the cylinder oscillating in the in-line direction and in the transverse direction are compared (Table 1) with the experimental results given by Tanida et al. (1973).

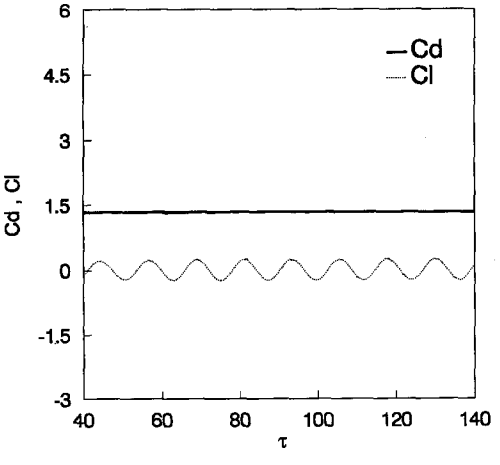

Fig. 3. Time dependent drag and lift of stationary cylinder ($Re = 100$, $F_n = 0.164$)

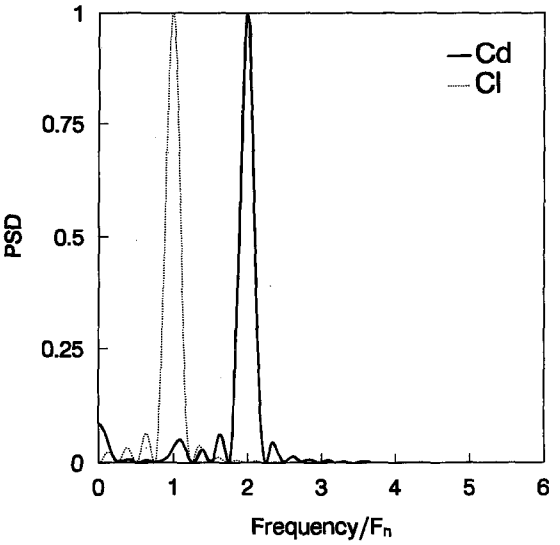

Fig. 4. Power spectra of the drag and lift force (stationary cylinder, $Re = 100$)

At a Reynolds number of 100, the computed value of Strouhal number ($F_n = 0.164$) agrees well with the experimental value of 0.166. The Strouhal number at a Reynolds number of 80 was calculated to be 0.157 which is in good agreement with the experimentally observed value of 0.154 (Roshko (1955)). It was also observed that the Strouhal numbers computed with a second order accurate time interpolation scheme were the same as those calculated with a first order accurate time differencing scheme.

The numerical model was also validated with the cylinder oscillating in the in-line and the transverse directions separately. In order to compare the numerical predictions with Tanida's experimental results, the position amplitude was set equal to $0.14D$ in both the in-line and transverse directions. The cylinder was forced to oscillate at twice the natural shedding frequency in the in-line direction and at a frequency equal to the natural shedding frequency in the transverse direction. Table 1 compares the computed values of mean drag and maximum lift with the experimental values given by Tanida et al. (1973). It can be observed that the mean drag values agree satisfactorily with the measured values of mean drag. A large discrepancy between the computed maximum lift and measured maximum lift has been observed in the case of flow past a stationary cylinder. This discrepancy may be attributed to the three dimensional nature of vortex shedding from a cylinder of finite length. Similar discrepancies were also observed in other computational investigations. In general, the numerical method used can be considered as valid.

In the following sections, the numerical results obtained at a Reynolds number of 100 with the cylinder oscillating in the in-line direction ($a_x = 0.2D$), transverse direction ($a_y = 0.2D$, $0.4D$ and $0.8D$) and combined in-line and transverse directions ($a_x = 0.2D$, $a_y = 0.2D$, $0.4D$ and $0.8D$) are discussed.

4.2
In-line oscillation

The lock-in range of frequency depends on the Reynolds number and the position amplitude of the cylinder. The maximum range of lock-in frequency is approximately ± 40 percent of the midpoint frequency (Griffin and Ramberg

Conditions	Mean drag computed	Mean drag measured (Tanida et al.)	Maximum lift computed	Maximum lift measured (Tanida et al.)
$Re = 80$ & stationary	1.379	1.3	0.23	0.08
$Re = 80$, $a_x = 0.14D$ & $F_x = 2F_n = 0.314$	1.5075	1.5	0.6577	0.5
$Re = 80$, $a_y = 0.14D$ & $F_y = F_n = 0.157$	1.4964	1.6	0.3239	-N/A-
$Re = 100$ & stationary	1.3241	1.25	0.2496	0.1

Table 1. Comparison of experimental and computational results

(1976)). Accordingly, the cylinder was forced to oscillate at frequencies such that the frequency parameters (F_x) were $1.2F_n$, $2F_n$ and $2.8F_n$). The frequency parameter $2F_n$ is the mid-point frequency where the lock-in should occur irrespective of the position amplitude of oscillation. Figure 5 shows the time history of drag and lift of the cylinder oscillating with a frequency parameter $F_x = 2F_n$ compared to $1.2F_n$ and $2.8F_n$. The mean drag, amplitude of drag and maximum lift are defined in Fig. 5. The variations of the mean drag, amplitude of the drag and maximum lift with the forced frequency of oscillation are depicted in Fig. 6. An higher mean drag and maximum lift were found with $F_x = 2F_n$. The amplitude of the drag increases with F_x. The power spectra of the drag and lift and lift are shown in Fig. 7. The dominant frequency component in all the drag variations is equal to the forcing frequency (Fig. 7(a)). The lift variations are always dominated by the frequency component equal to the Strouhal frequency (F_n) (Fig. 7(b)). This indicates that lock-in occurs at $F_x = 2F_n$ only. Previously, other researchers have reported that an increase in the position amplitude of oscillation widens the lock-in frequency range of oscillation. Additional frequency components in the lift variations are due to the changes in the vortex shedding process from the cylinder oscillating in the in-line direction. The dominant frequency components in the drag and lift variations are listed in Table 2. Figure 8 shows the

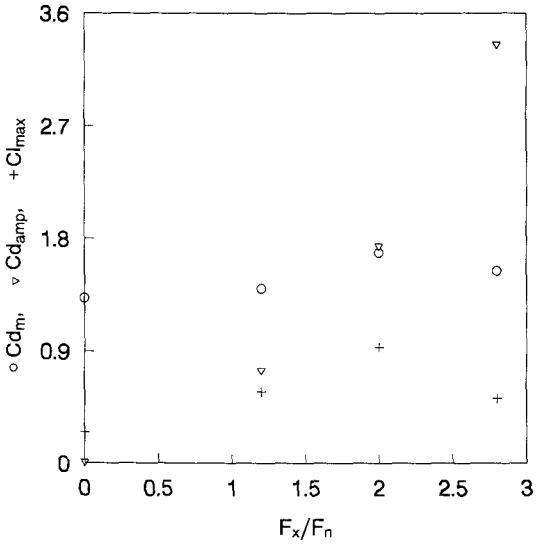

Fig. 6. Forcing frequency vs mean drag, amplitude of drag and maximum lift (in-line oscillation, $a_x = 0.2D$)

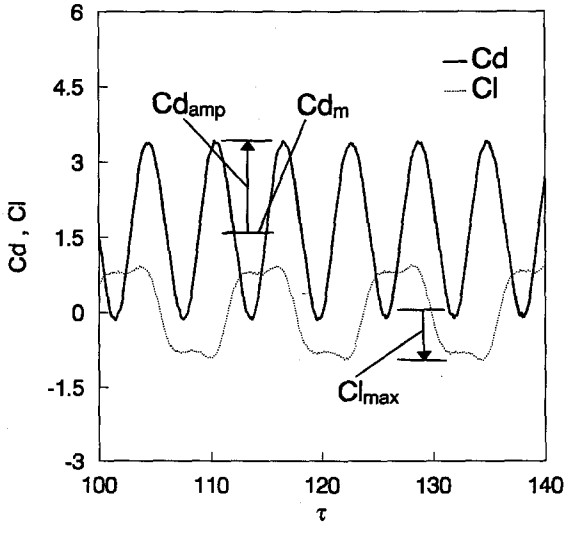

Fig. 5. Time dependent drag and lift (in-line oscillation, $a_x = 0.2D$, $F_x = 2F_n$)

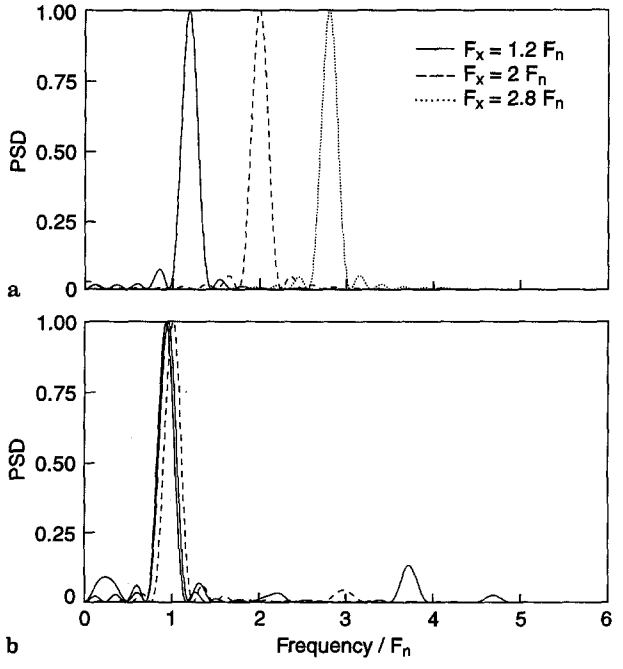

Fig. 7a,b. Power spectra of the forces a drag b lift (in-line oscillation, $a_x = 0.2D$)

Table 2. Summary of dominant frequency components (In-line oscillation, $a_x = 0.2D$)

F_x	Frequency components Cd	Frequency components Cl
0	$2F_n$	F_n
$1.2F_n$	$1.2F_n$	F_n
$2F_n$	$2F_n$	F_n, $3F_n$
$2.8F_n$	$2.8F_n$	F_n, $3.73F_n$

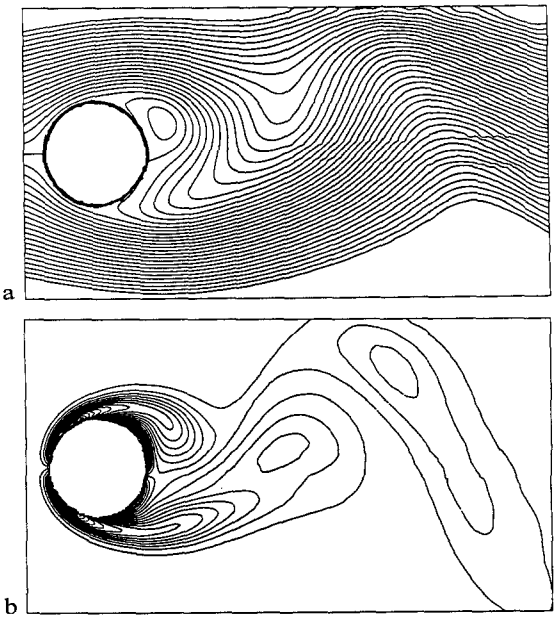

Fig. 8a,b. Contour maps of a stream function b vorticity (in-line oscillation, $a_x = 0.2D$, $F_x = 2F_n$)

contour maps of the stream function and the vorticity at the same instant of time. At this time, the oscillating cylinder has a zero velocity.

4.3 Transverse oscillation

In the case of transverse oscillation, the cylinder was forced to oscillate at frequencies such that the frequency parameters (F_y) were $0.6F_n$, F_n and $1.4F_n$. The frequency parameter $F_y = F_n$ is the mid-point frequency where the lock-in should occur irrespective of the position amplitude of oscillation. The time history of the drag and lift of the cylinder with the frequency parameter $F_y = F_n$ and position amplitudes of $0.2D$, $0.4D$ and $0.8D$, are depicted in Figs. 9(a), 9(b) and 9(c) respectively. In these figures, the variations of the amplitude of the drag and maximum lift with the position amplitude at the mid-point lock-in frequency can be observed. In order to quantify the observations, Figs. 10(a), 10(b) and 10(c) show the mean drag, amplitude of drag and maximum lift at different forcing frequencies and position amplitudes of oscillation. Figure 10(a) shows that, for $a_y = 0.2D$ and $0.4D$, the predicted mean drag attains a maximum value between $F_y = 0.6F_n$ and $F_y = 1.4F_n$. In the case of $a_y = 0.8D$, the mean drag increases with frequency of oscillation. The computed mean drag for $F_y = 1.4F_n$ is

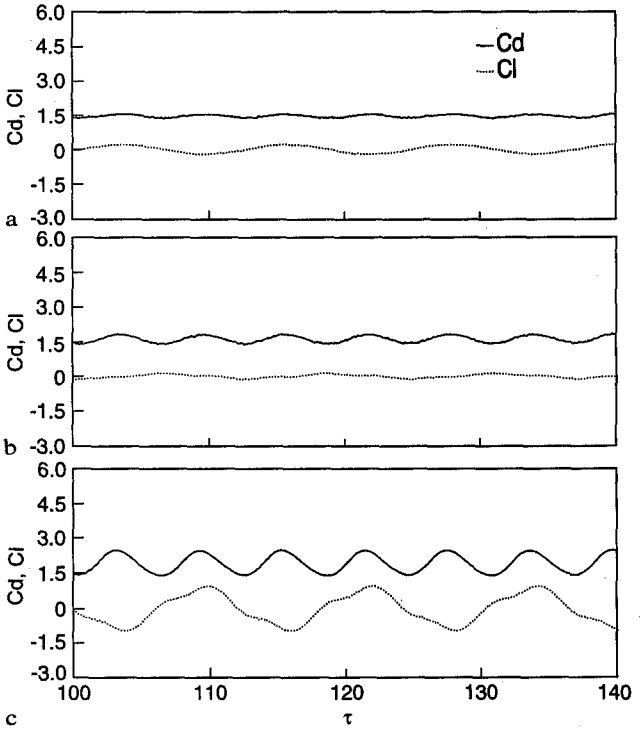

Fig. 9a–c. Time dependent drag and lift (transverse oscillation, $F_y = F_n$) a $a_y = 0.2D$ b $a_y = 0.4D$ c $a_y = 0.8D$

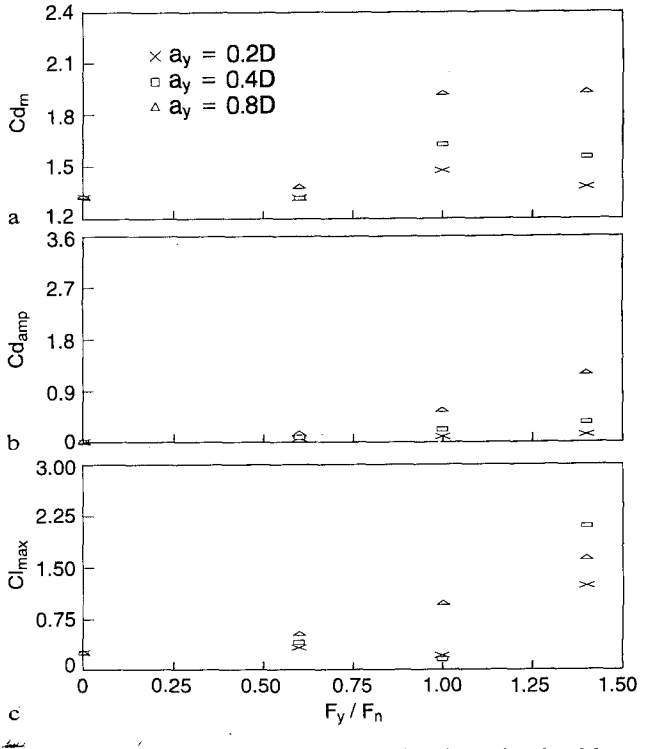

Fig. 10a–c. Forcing frequency vs a mean drag b amplitude of drag c maximum lift (transverse oscillation)

marginally higher than for $F_y = F_n$. The mean drag increases with the position amplitude at all the frequencies of oscillation. The amplitude of the drag (Fig. 10(b)) increases with both the frequency of oscillation and the position amplitude. For $a_y = 0.2D$ and $0.4D$, the maximum lift (Fig. 10(c)) attains

a minimum value between $F_y = 0.6F_n$ and $F_y = 1.4F_n$. In the case of $a_y = 0.8D$, the maximum lift continually increases with the frequency of oscillation.

The power spectra of the drag with $a_y = 0.2D$ (Fig. 11(a)) show that the dominant frequency component is $2F_n$ for $F_y = 0.6F_n$ and $F_y = F_n$. With $F_y = 1.4F_n$, the dominant frequencies are $2.8F_n$ and $2F_n$ indicating the influence of forcing frequency on the drag at frequencies higher than the mid-point lock-in frequency. The existence of a frequency component F_n in the drag variation at $F_y = 0.6F_n$ and $F_y = 1.4F_n$ implies that the lock-in does not occur at these forcing frequencies. With $a_y = 0.4D$ (Fig. 11(b)), the dominant frequencies in the drag are associated only with the forcing frequency of oscillation at $F_y = F_n$ and $F_y = 1.4F_n$. Hence, the lock-in occurs at both $F_y = F_n$ and $F_y = 1.4F_n$. With $F_y = 0.6F_n$, the power spectra of the drag also contains a frequency component $2F_n$ in addition to $1.2F_n$ indicating that the lock-in does not occur at this frequency of oscillation. With $a_y = 0.8D$ (Fig. 11(c)), the dominant frequencies in the drag are associated only with forcing frequency at all the chosen frequency parameters of oscillation. This means that all the selected forcing frequencies of oscillation fall within the lock-in range of frequency. The power spectra of the lift with $a_y = 0.2D$ (Fig. 12(a)) show that the dominant frequency component is F_n at $F_y = 0.6F_n$ and $F_y = F_n$. The forcing frequency of oscillation, however, dominates over the Strouhal frequency at $F_y = 1.4F_n$. The power spectra of the lift with $a_y = 0.4D$ (Fig. 12(b)) indicates that the forcing frequency is dominant at all the frequencies of oscillation. With $a_y = 0.4D$ and $F_y = 0.6F_n$, the forcing frequency is marginally more dominant than F_n. It is evident from the power spectra of the lift at $a_y = 0.8D$ (Fig. 12(c)) that the frequency components in the lift are attributed only to the forcing frequency oscillation. Table 3 gives the summary of dominant frequency components in the time-dependent drag and lift at different position amplitudes. With $F_y = F_n$ and $a_y = 0.2D$, contour maps of the stream function and the vorticity at the time of zero velocity of the oscillating cylinder are shown in Fig. 13. A comparison of Figs. 8(a) and 13(a) shows that the separation region the case of transverse oscillation is smaller than that of the in-line oscillation.

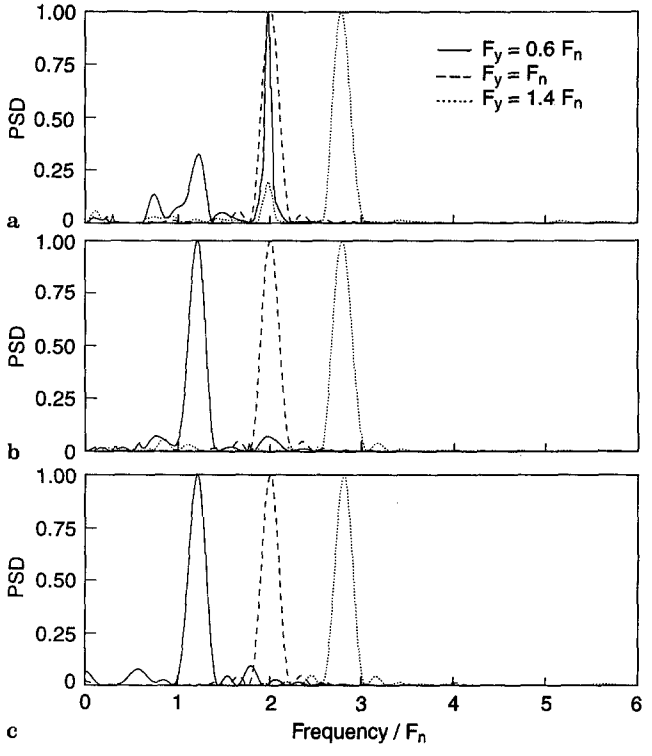

Fig. 11a–c. Power spectra of the drag forces (transverse oscillation) **a** $a_y = 0.2D$ **b** $a_y = 0.4D$ **c** $a_y = 0.8D$

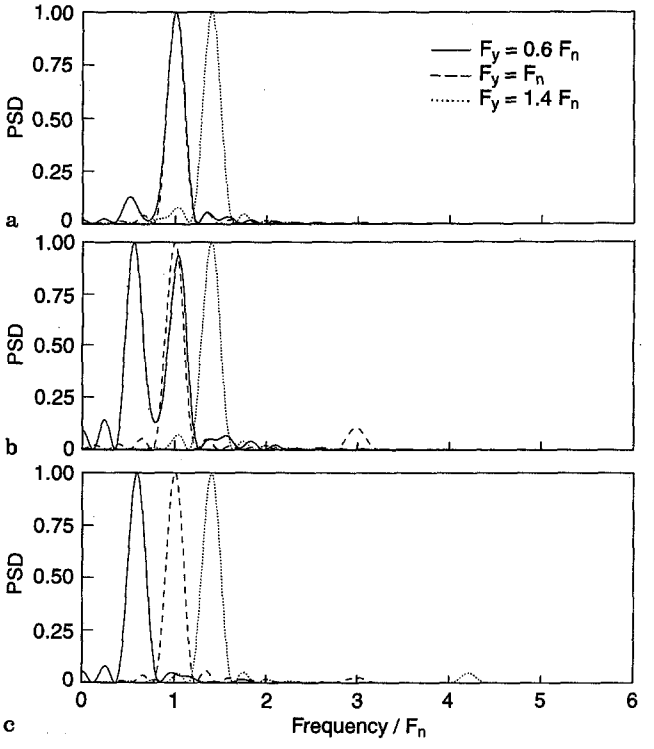

Fig. 12a–c. Power spectra of the lift forces (transverse oscillation) **a** $a_y = 0.2D$ **b** $a_y = 0.4D$ **c** $a_y = 0.8D$

F_y	Frequency components $a_y = 0.2D$		Frequency components $a_y = 0.4D$		Frequency components $a_y = 0.8D$	
	Cd	Cl	Cd	Cl	Cd	Cl
0	$2F_n$	F_n	$2F_n$	F_n	$2F_n$	F_n
$0.6F_n$	$1.2F_n$, $2F_n$	$0.6F_n$, F_n	$1.2F_n$, $2F_n$	$0.6F_n$, F_n	$1.2F_n$	$0.6F_n$
F_n	$2F_n$	F_n	$2F_n$	F_n, $3F_n$	$2F_n$	F_n
$1.4F_n$	$2F_n$, $2.8F_n$	F_n, $1.4F_n$	$2.8F_n$	$1.4F_n$	$2.8F_n$	$1.4F_n$

Table 3. Summary of dominant frequency components (Transverse oscillation)

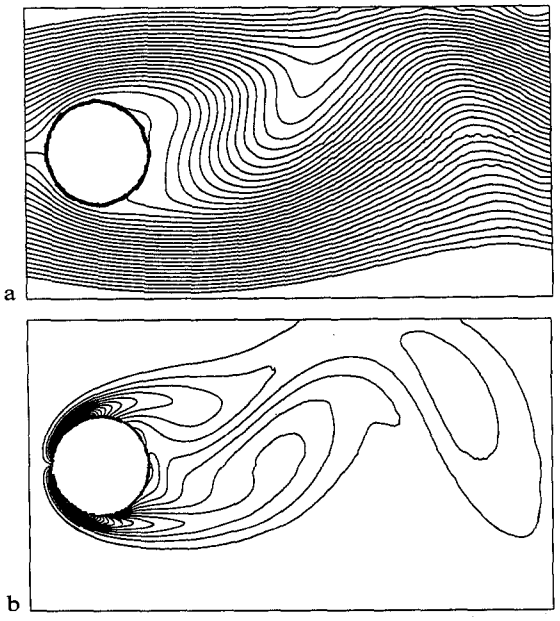

Fig. 13a,b. Contour maps of a stream function b vorticity (transverse oscillation, $a_y = 0.2D$, $F_y = F_n$)

4.4 Combined oscillation

The cylinder was forced to oscillate simultaneously in the in-line and transverse directions with the following combinations of frequency parameters: $F_x = 2F_y = 1.2F_n$, $F_x = 2F_y = 2F_n$ and $F_x = 2F_y = 2.8F_n$. The position amplitude in the in-line direction (a_x) was set equal to $0.2D$. In the transverse direction, the cylinder was forced to oscillate with three different position amplitudes (a_y): $0.2D$, $0.4D$ and $0.8D$. Figures 14(a), 14(b) and 14(c) show the time dependent drag and lift with $F_x = 2F_n$ and $F_y = F_n$, at three different combinations of position amplitudes in the in-line and transverse directions. The lift variation is very much different than a sinusoidal variation. It contains several frequency components. At the mid-point lock-in frequency, the variations of the amplitude of the drag and maximum lift at different combinations of position amplitudes can be observed in these figures. In order to quantify these observations, the mean drag, the amplitude of drag and maximum lift at different forcing frequencies of the oscillating cylinder are depicted in Figs. 15(a), 15(b) and 15(c). With $a_y = 0.2D$ and $0.4D$ (Fig. 15(a)), the predicted mean drag attains a maximum value at $F_y = F_x/2 = F_n$. In the case of $a_y = 0.8D$, the mean drag increases with frequency of oscillation, however, the computed mean drag for $F_y = F_x/2 = 1.4F_n$ is only marginally higher than for $F_y = F_n$. The mean drag increases with the position amplitude at all the frequencies of oscillation. This is similar to what happened in the case of transverse oscillation, however, the mean drag is higher for combined oscillation at all the forcing frequencies and position amplitudes of oscillation studied. At smaller position amplitudes, the mean drag variation with the frequency of oscillation (Figs. 6, 10(a) and 15(a)) is very similar to the case of in-line oscillation and transverse oscillation. The amplitude of the drag (Fig. 15(b)) increases with the frequency of oscillation. Unlike in the case of transverse oscillation, the influence of position amplitude of oscillation in the transverse direction on the amplitude of the drag is negligible. The maximum lift (Fig. 15(c)) increases with both the position amplitude and the forcing frequency of oscillation.

The power spectra of the drag (Figs. 16(a), 16(b) and 16(c)) show that the dominant frequency components are associated only with the forcing frequency of oscillation. Similar spectral

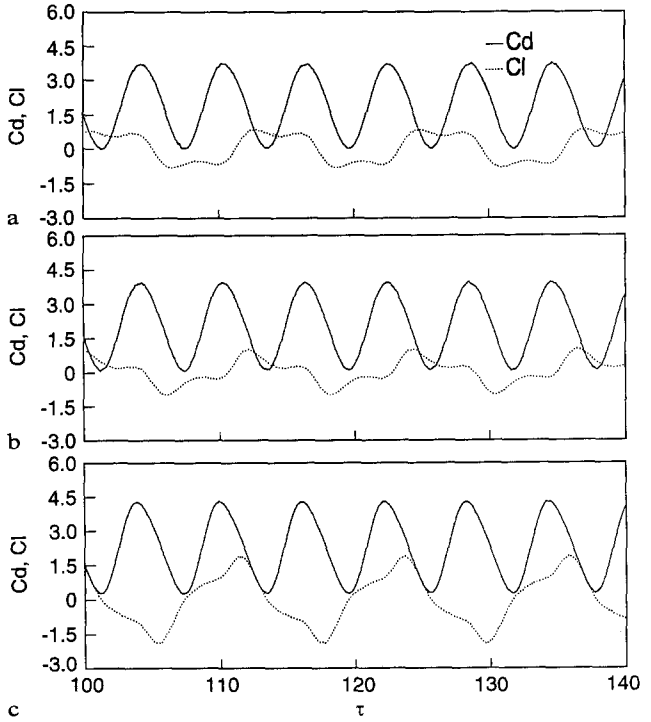

Fig. 14a–c. Time dependent drag and lift (combined oscillation, $F_y = F_x/2 = F_n$) **a** $a_x = a_y = 0.2D$ **b** $a_x = 0.2D$, $a_y = 0.4D$ **c** $a_x = 0.2D$, $a_y = 0.8D$

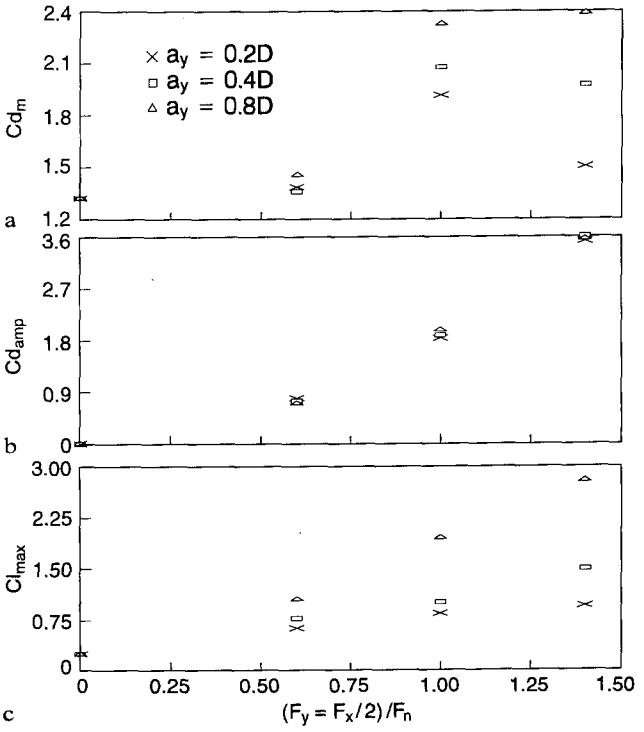

Fig. 15a–c. Forcing frequency vs **a** mean drag **b** amplitude of drag **c** maximum lift (combined oscillation, $a_x = 0.2D$)

characteristics are observed in the case of in-line oscillation. The position amplitude of oscillation in the transverse direction does not influence the spectral characteristics of the drag variation. As in the case of transverse oscillation, the power spectra of the lift with $a_x = a_y = 0.2D$ (Fig. 17(a)) show that the dominant frequency component is F_n at $F_y = F_x/2 = 0.6F_n$ and $F_y = F_x/2 = F_n$. This implies that the lock-in does not occur at $F_y = F_x/2 = 0.6F_n$. In the case of $F_y = F_x/2 = 1.4F_n$, the forcing frequency of oscillation is dominant in the lift variation. The absence of the frequency component F_n in the lift variation for $F_y = F_x/2 = 1.4F_n$ means that lock-in occurs. The power spectra of the lift for $a_y = 0.4$D (Fig. 17(b)) indicates that the forcing frequency of oscillation is dominant at all the frequencies of oscillation as opposed to the $a_y = 0.2D$ case. With $a_y = 0.4D$ and $F_y = 0.6F_n$, the frequency component F_n is less dominant than $0.6F_n$. However, the existence of the frequency component F_n in the lift variation implies that complete lock-in does not occur at $F_y = F_x/2 = 0.6F_n$. It is evident from the power spectra of the lift at $a_y = 0.8D$ (Fig. 17(c)) that the frequency components in the lift are attributed only to the forcing frequency of oscillation. This indicates that all the selected forcing frequencies of oscillation fall within in the lock-in range of frequency. Table 4 gives the summary of the dominating frequency components in the lift and drag at three different combinations of position amplitudes of oscillation of the cylinder. At the mid-point lock-in frequency ($F_y = F_x/2 = F_n$), Fig. 18 depicts the contour maps of the stream function and the vorticity at the time of zero velocity of the oscillating cylinder in the in-line and the transverse directions. A comparison of Figs. 13(b) and 18(b) indicates that the diffusion of vorticity is greater in the case of transverse oscillation than the combined oscillation.

5 Conclusions

The following conclusions are drawn from the present numerical simulation of a flow past an oscillating cylinder.

In-line oscillation: Lock-in is observed at $F_x = 2F_n$. At this frequency, the maximum lift is predicted to be 3.7 times the maximum lift for the case of flow past a stationary cylinder. An additional component of frequency equal to $3F_n$ exists in the lift variation.

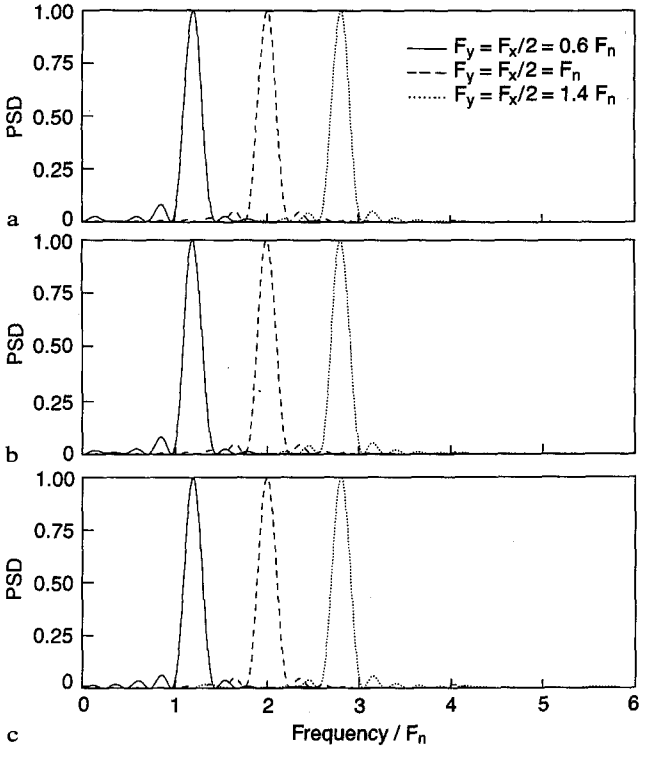

Fig. 16a–c. Power spectra of the drag forces (combined oscillation) **a** $a_x = a_y = 0.2D$ **b** $a_x = 0.2D$, $a_y = 0.4D$ **c** $a_x = 0.2D$, $a_y = 0.8D$

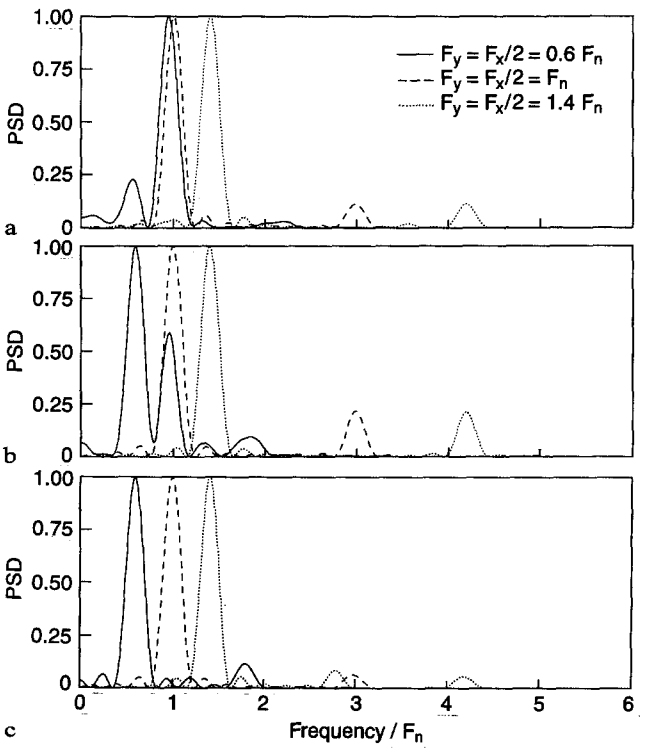

Fig. 17a–c. Power spectra of the lift forces (combined oscillation) **a** $a_x = a_y = 0.2D$ **b** $a_x = 0.2D$, $a_y = 0.4D$ **c** $a_x = 0.2D$, $a_y = 0.8D$

$F_x =$ $2F_y$	Frequency components $a_x = a_y = 0.2D$		Frequency components $a_x = 0.2D$, $a_y = 0.4D$		Frequency components $a_x = 0.2D$, $a_y = 0.8D$	
	Cd	Cl	Cd	Cl	Cd	Cl
0	$2F_n$	F_n	$2F_n$	F_n	$2F_n$	F_n
$1.2F_n$	$1.2F_n$	$0.6F_n$, F_n	$1.2F_n$	$0.6F_n$, F_n, $1.8F_n$	$1.2F_n$	$0.6F_n$, $1.8F_n$
$2F_n$	$2F_n$	F_n, $3F_n$	$2F_n$	F_n, $3F_n$	$2F_n$	F_n, $3F_n$
$2.8F_n$	$2.8F_n$	$1.4F_n$, $4.2F_n$	$2.8F_n$	$1.4F_n$, $4.2F_n$	$2.8F_n$	$1.4F_n$, $2.8F_n$, $4.2F_n$

Table 4. Summary of dominant frequency components (Combined oscillation)

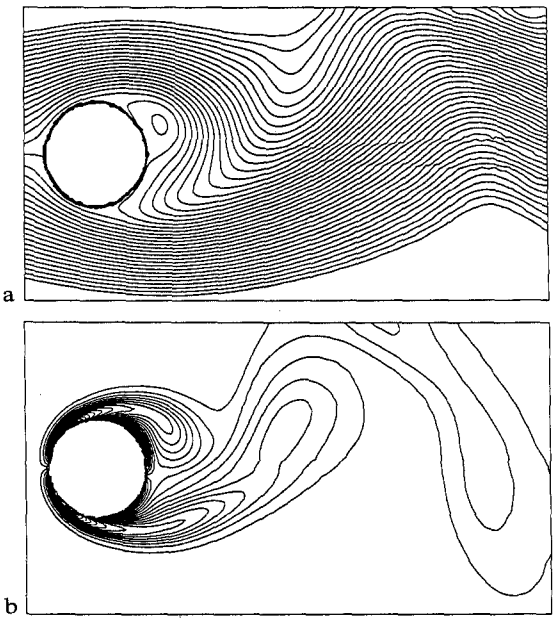

Fig. 18a,b. Contour maps of **a** stream function **b** vorticity (combined oscillation, $a_x = a_y = 0.2D$, $F_y = F_x/2 = F_n$)

Transverse oscillation: The mean drag and the amplitude of drag increase with the position amplitude of the oscillating cylinder. With $a_y = 0.2D$ and $a_y = 0.4D$, the maximum lift attains a minimum value at $F_y = F_n$. The lock-in range of frequency widens at higher position amplitudes in the transverse direction. With $a_y = 0.2D$, the dominant frequency components in the drag and lift variations are associated with the forcing frequency and the natural shedding frequency. At higher position amplitudes, the dominant frequencies in the drag and lift variations are associated only with the forcing frequency of the cylinder oscillation and the lock-in occurs at all the chosen frequency parameters.

Combined oscillation: The mean drag and the maximum lift increase with the position amplitude in the transverse direction. The influence of the position amplitude in the transverse direction on the amplitude of drag is negligible. As in the case of transverse oscillation, the lock-in range of frequency increases with the position amplitude of the cylinder oscillating in the transverse direction. With $F_x = 2F_y = 2.8F_n$, the frequency components in the drag and lift variations are associated only with forcing frequency at all the selected position amplitudes of oscillation. At higher position amplitudes in the transverse direction, the lift force contains additional frequency components. The present study gives a better understanding of the effects of lock-in with combined oscillation on the mean drag, amplitude of drag, maximum lift and the frequency components in the drag and lift variations.

References

Bearman, P. W.; Obasaju 1989: Transverse forces on a circular cylinder oscillating in-line with a steady current. Proc. Eighth Int. Conf. on Offshore Mechanics and Arctic Engineering. Hague, 253–258

Bublitz, P. 1972: Unsteady pressures and forces acting on an oscillating circular cylinder in transverse flow. Flow Induced Structural Vibrations Symposium, Karlseruhe, Germany, 443–453

Chilukuri, R. 1987: Incompressible laminar flow past a transversely vibrating cylinder. ASME. J. Fluids Engg. 109: 166–171

Griffin, O. M.; Ramberg, S. E. 1974: The vortex-street wakes of vibrating cylinders. J. Fluid Mech. 66: 553–576

Griffin, O. M.; Ramberg, S. E. 1976: Vortex shedding from a cylinder vibrating in line with an incident uniform flow. J. Fluid Mech. 75: 257–271

Hurlbut, S. E.; Spaulding, M. L.; White, F. M. 1982: Numerical solution for laminar two dimensional flow about a cylinder oscillating in a uniform stream. ASME J. Fluids Engg. 104: 214–222

Jordan, S. K.; Fromm, J. E. 1972: Oscillatory drag, lift and torque on a circular cylinder in a uniform flow. Phys. Fluids 15: 371–376

Lecointe, Y.; Piquet, J. 1989: Flow structure in the wake of an oscillating cylinder. ASME J. Fluids Engg. 111: 139–148

Li, J.; Sun, J.; Roux, B. 1992: Numerical study of an oscillating cylinder in uniform flow and in the Wake of an upstream cylinder. J. Fluid. Mech. 237: 457–478

Mittal, S.; Tezduyar, T. E. 1992: A finite element study of incompressible flows past oscillating cylinders and aerofoils. Int. J. Num. Methods in Fluids 15: 1073–1118

Moe, G.; Wu, Z. J. 1989: The lift force on a vibrating cylinder in a current. Proc. Eighth Int. Conf. on Offshore Mechanics and Arctic Engineering, Hague, 159–268

Rao, P. M.; Kuwahara, K.; Tsuboi, K. 1992: Computational study of unsteady viscous flow around a transversely and longitudinally oscillating circular cylinder in a uniform flow at high Reynolds numbers. Computational Mechanics 10: 414–428

Roshko, A. 1955: On the wake and drag of bluff bodies. J. Aero. Science, 22: 124–135

Son, J. S.; Hanratty, T. J. 1969: Numerical solution for the flow around a cylinder at Reynolds numbers of 40, 200 and 500. J. Fluid Mech. 35: 369–386

Stansby, P. K. 1976: The locking-on of vortex shedding due to the cross-stream vibration of circular cylinders in uniform and shear flows. J. Fluid Mech. 74: 641–665

Ta Phuoc Loc; Bouard, R. 1985: Numerical solution of the early stage of the unsteady viscous flow around a circular cylinder: a comparison with experimental visualization and measurements. J. Fluid Mech. 160: 93–117

Tanaka, H.; Takahara, S. 1969: Study on unsteady aerodynamic forces acting on an oscillating cylinder. Proc. Nineteenth Japan National Congress for Appl. Mech., Tokyo, 162–166

Tanida, Y.; Okajima, A.; Watanabe, Y. 1973: Stability of a circular cylinder oscillating in uniform flow or in a wake. J. Fluid Mech. 61: 769–784

Triantafyllou, G. S.; Karniadakis, G. E. 1989: Forces on a vibrating cylinder in steady cross flow. 8th International Conference on Offshore Mechanics and Arctic Engineering, Hague, 247–251

Tsuboi, K.; Tamura, T.; Kuwahara, K. 1988: Numerical simulation of unsteady flow patterns around a vibrating cylinder. AIAA Paper No. 88-0128, Reno